Journal of the Mechanical Behavior of Biomedical Materials 82 (2018) 320–328

Contents lists available at ScienceDirect

Journal of the Mechanical Behavior of Biomedical Materials

journal homepage: www.elsevier.com/locate/jmbbm

Swelling of fiber-reinforced soft tissues is affected by fiber orientation, fiber stiffness, and lamella structure

Bo Yang[a], Grace D. O'Connell[a,b,*]

[a] Department of Mechanical Engineering, University of California, Berkeley, United States
[b] Department of Orthopaedic Surgery, University of California, San Francisco, United States

ARTICLE INFO

Keywords:
Fiber-reinforced soft tissue
Swelling
Fiber orientation
Intervertebral disc

ABSTRACT

Native and engineered fiber-reinforced tissues are composites comprised of stiff collagen fibers embedded within an extrafibrillar matrix that is capable of swelling by absorbing water molecules. Tissue swelling is important for understanding stress distributions between collagen fibers and extrafibrillar matrix, as well as for understanding mechanisms of tissue failure. The swelling behavior of fiber-reinforced tissues in the musculoskeletal system has been largely attributed to the glycosaminoglycan content. Recent work demonstrated anisotropy in the swelling response of the annulus fibrosus in the intervertebral disc. It is well known that collagen fiber orientation affects elastic behavior, but the effect of collagen fiber network on tissue swelling behavior is not well understood. In this study, we developed three series of models to evaluate the effect of collagen fiber orientation, fiber network architecture (*i.e.*, single or multi-fiber families within a layer), and fiber stiffness on bulk tissue swelling, which was simulated by describing the extrafibrillar matrix as a triphasic material, as proposed by Lai *et al.* Model results were within one standard deviation of reported mean values for changes in tissue volume, width, and thickness under free swelling conditions. The predicted swelling response of single-fiber family structures was highly dependent on fiber orientation and the number of lamellae in the bulk tissue. Moreover, matrix swelling resulted in tissue to twist, which reduced fiber deformations, demonstrating a balance between fiber deformation and matrix swelling. Large changes in fiber stiffness (20 × increase) had a relatively small effect on tissue swelling (~ 2% decrease in swelling). In conclusion, fiber angle, fiber architecture (defined as single- *versus* multiple fiber families in a layer), and the number of layers in a single fiber family structure directly affected tissue swelling behavior, including fiber stretch, fiber reorientation, and tissue deformation. These findings support the need to develop computational models that closely mimic the native architecture in order to understand mechanisms of stress distributions and tissue failure.

1. Introduction

Native and engineered fiber-reinforced tissues, such as the annulus fibrosus (AF), arterial walls, tendons, ligaments, and cartilage, are composite structures that include stiff collagen fibers embedded within an extrafibrillar matrix (Lemaitre, 2001; O'Connell et al., 2009; Rumian et al., 2007; Wang et al., 2016). Many of these tissues have an excellent capacity to absorb water from the surrounding environment because of the glycosaminoglycans (GAGs) in the extrafibrillar matrix, which is essential for fibril sliding during loading (Azeloglu et al., 2008; Fung, 1991; Screen et al., 2006; Żak and Pezowicz, 2016). Fiber-reinforced tissues display a wide range of fiber orientations depending on the stresses experienced *in situ* (Cassidy et al., 1989; Rumian et al., 2007), resulting in anisotropy of bulk tissue mechanical properties and swelling behavior (Elliott and Setton, 2001; Żak and Pezowicz, 2016). However, the effect of the collagen fiber network on bulk tissue swelling response is not well understood. As biological repair strategies aim to recapitulate the mechanical behavior of healthy native tissues, elucidating the effect of fiber architecture on swelling behavior is important for understanding stress distributions between subcomponents.

There has been extensive research evaluating the role of collagen fiber orientation on elastic mechanical properties (Abraham et al., 2011; Elliott and Setton, 2001; Lynch et al., 2003; Meng et al., 2017; Shirazi and Shirazi-Adl, 2008). Differences in tissue mechanics arise from differences in fiber orientation, fiber architecture complexity, and other secondary constituents (*e.g.*, elastin and types of collagen fibers) (Cassidy et al., 1989; Eyre and Muir, 1976). That is, tissues with highly aligned collagen fibers have significant anisotropy and are stiffer than tissues with fibers aligned off-axis from the primary loading direction (Elliott and Setton, 2001; Lynch et al., 2003). Moreover, constitutive

* Correspondence to: Department of Mechanical Engineering, University of California, Berkeley, 5122 Etcheverry Hall, #1740, Berkeley, CA 94720, United States.
E-mail address: g.oconnell@berkeley.edu (G.D. O'Connell).

https://doi.org/10.1016/j.jmbbm.2018.03.039
Received 7 February 2018; Received in revised form 13 March 2018; Accepted 29 March 2018
Available online 03 April 2018
1751-6161/ © 2018 Elsevier Ltd. All rights reserved.

models of the AF showed that fiber-matrix interactions act to maintain bulk tissue tensile mechanical behavior with degeneration (O'Connell et al., 2009; Wagner and Lotz, 2004). However, there has been limited research investigating the role of the extrafibrillar matrix, which accounts for 75–95% of the tissue's wet-weight (*i.e.*, GAGs plus water) (Adams, 2004; Cortes and Elliott, 2012; Lin et al., 2004).

The role of GAGs and tissue swelling is of particular interest for understanding stress distributions between collagen fibers and the extrafibrillar matrix, as well as for understanding mechanisms of tissue failure (Wood et al., 1998). For example, the intervertebral disc is complex organ comprised of distinct fibro-cartilaginous materials, including the nucleus pulposus, which is surrounded by the AF. Differences in biochemical composition and architecture contribute to differences in swelling response of explants from the two regions, which, in turn, altered joint-level mechanical behavior (Bezci and O'Connell, 2017; Bezci et al., 2015; Żak and Pezowicz, 2016). The swelling capacity of AF explants was shown to be approximately 70% of nucleus pulposus explants (Bezci et al., 2015). Moreover, AF swelling, similar to mechanical properties, is highly anisotropic, with more swelling occurring in the radial direction (21 ± 4%) than the axial (14 ± 6%) or circumferential directions (−2 ± 4%) (Żak and Pezowicz, 2016). Large direction-dependent swelling deformations have also been observed in cervical tissue during pregnancy and cardiovascular vessels with disease (Roccabianca et al., 2014; Yoshida et al., 2016).

While multiple studies have reported the swelling behavior of various fiber-reinforced tissues, it is difficult to compare findings and discern the role of fiber orientation on tissue swelling, due to other differences in tissue composition. Computational models provide a powerful tool for understanding the role of matrix swelling on bulk tissue behavior. However, many finite element models of fiber-reinforced tissues rely on hyperelastic material descriptions, which do not include fluid-dependent behaviors and cannot elucidate the role of fiber-matrix interactions (Guerin and Elliott, 2007; Holzapfel et al., 2000). The triphasic mixture theory, originally proposed by Lai *et al.*, can be used to describe material deformations as a combination of fiber stretch, elastic deformations from the extrafibrillar matrix, and osmotic pressure (Lai et al., 1991). This approach has been successful in describing cartilage mechanics and swelling of engineered cartilage constructs (Abazari et al., 2009; Ateshian et al., 2004).

Thus, the objective of this study was to determine the effect of collagen fiber orientation and fiber network complexity on tissue swelling behavior and resulting deformations from osmotic loading. We developed a series of tissue-level finite element models that represents specimen orientations commonly used for uniaxial tensile testing (Acaroglu et al., 1995; Green et al., 1993; O'Connell et al., 2009, 2012). Material parameters for the models were determined by curve-fitting experimental data from the AF; however, the overall observations, with respect to fiber orientation and tissue swelling, are applicable to other fiber-reinforced tissues. The findings from these models highlight difficulties in comparing mechanical properties between studies, where the stated reference configuration may vary significantly depending on hydration conditions (Han et al., 2012; Żak and Pezowicz, 2016).

2. Methods

2.1. Model geometry and mesh

Three series of models were developed (Table 1). Models in Series I evaluated the effect of multi-lamella structures on tissue swelling, where each layer included a single fiber-family population with a defined orientation. Fiber orientation in adjacent layers alternated about the z-axis (Fig. 1A). Single and multi-lamella structures were evaluated, including models with 1-, 2-, 3-, 4-, or 6-layers (Fig. 1C–G). Models in Series II evaluated the effect of multiple fiber families in single lamellae on bulk tissue swelling behavior (Fig. 1B). For this study, we limited the analysis to a two-fiber family description. Models in Series III evaluated the effect of fiber stiffness on tissue swelling by simulating a 20-fold increase in fiber stiffness. Therefore, nine separate fiber network configurations were evaluated (Table 1).

Table 1
Nine fiber network configurations were developed. In Series I the effect of multi-lamellae structures on bulk tissue swelling was evaluated (single fiber family description). Series II investigated the effect of a two-fiber family description on tissue swelling. Series III evaluated the effect of fiber stiffness on tissue swelling.

	Fiber property	Model
Series I	Alternating fiber orientation	1-layer
		2-layer
		3-layer
		4-layer
		6-layer
Series II	2 family	2-layer, 2 fiber family
		3-layer, 2 fiber family
Series III	20 × stiffer	3-layer, stiffer fibers
		3-layer, 2 fiber family, stiffer fibers

All models were developed and meshed in Preview 1.19.0 (FEBio Preprocessor, febio.org) (Maas et al., 2012). Lamellae dimensions in the reference configuration were 2 mm, 0.2 mm, and 10 mm for the width, thickness, and length, respectively (~ 24,000 hexahedral elements per lamella). Lamellae thickness was chosen based on the average AF lamellae thickness (Cassidy et al., 1989), and the length and width were selected based on ASTM standards for uniaxial test specimens (aspect ratio = 5) (Standard, 2004).

Fibers were orientated between 0° and 90° with respect to the vertical axis (Fig. 1C - θ). The effect of fiber orientation was assessed in increments of 15° for each model. Thus, models with fibers oriented at 0° represented the fiber orientation observed in tendons and ligaments tested along the longitudinal direction, while the 90° models mimicked the fiber orientation of tendons or ligaments tested in the transverse direction. Models with fibers oriented between 30° and 60° were developed to replicate fiber orientation of the AF (Cassidy et al., 1989; Kannus, 2000). A 'No-Fiber' case was developed as a control case. Therefore, a total of 72 models were developed (8 fiber orientations x 9 fiber network configurations).

2.2. Material properties

Triphasic mixture theory was used to describe the tissue as a combination of three phases: a solid phase and two fluid phases (water and monovalent ions) (Ateshian et al., 2004; Lai et al., 1991; Maas et al., 2012). The solid phase (Eq. (1)) consisted of the extrafibrillar matrix (Eqs. 2–4) and nonlinear fibers (Eqs. 5–8), where W_i represented strain energy functions (Maas et al., 2012). The extrafibrillar matrix was defined as a compressible hyperelastic material using the Holmes-Mow description (Eq. (2)). Matrix material properties were assumed to be spatially uniform throughout the tissue and consistent across all models. Material coefficients (E_m, ν, and β) were selected based on values reported in the literature (Table 2) (Cortes et al., 2014).

$$W = W_{matrix} + W_{fiber} \tag{1}$$

$$W_{matrix}(I_1, I_2, J) = \frac{1}{2}c(e^{Q}-1) \tag{2}$$

where Q and c were expressed as:

$$Q = \frac{\beta}{\lambda+2\mu}[(2\mu - \lambda)(I_1-3) + \lambda(I_2-3) - (\lambda+2\mu)lnJ^2] \tag{3}$$

$$c = \frac{\lambda+2\mu}{2\beta} \tag{4}$$

I_1 and I_2 are the first and second invariants of the right Cauchy-Green deformation tensor, $\mathbf{C}$ ($\mathbf{C} = \mathbf{F}^T\mathbf{F}$), J is the Jacobian of the

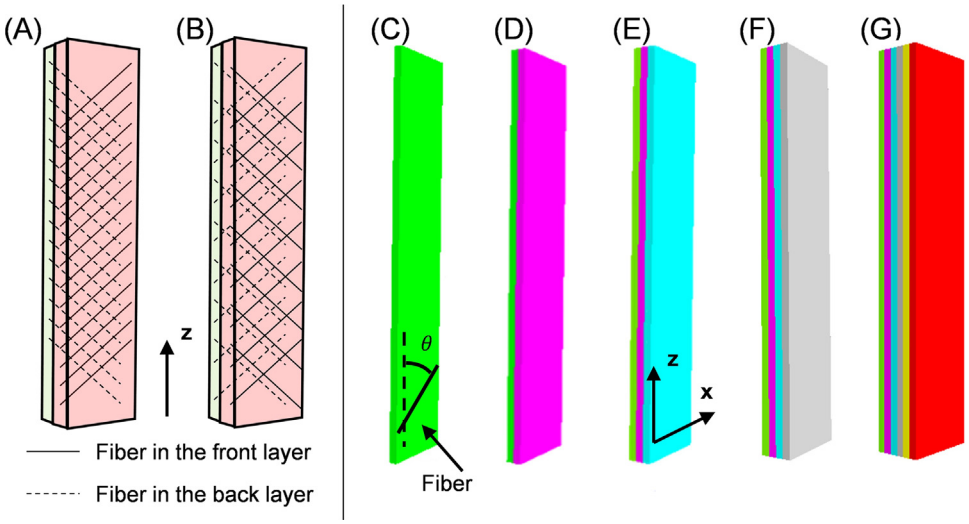

Fig. 1. In Series I, each layer consisted of a single fiber-family population, where fiber orientation alternated about the z-axis between layers (A). In Series II, each layer consisted of two-fiber family populations with each population alternating about the z-axis (B). Multi-lamella structures were developed for Series I (C-G). **Note**: A multi-layer description does not alter the response for a two-layer fiber family description.

Table 2
Material parameters used in all models. E_m: Extrafibrillar matrix modulus, υ: Poisson ratio, β: non-linear parameter for the Holmes-Mow description, E_f: collagen fiber modulus (*E_f = 23 for each fiber family in Series II, E_f = 920 for single-fiber family description in Series III, and E_f = 460 for the 2-fiber family description in Series III (Table 1).), γ: exponential term for the toe-region response of the fibers, I_0: square of the stretch ratio between the toe- and linear-region, ϕ_0: tissue solid fraction, k_0: hydraulic permeability in the reference configuration, M: nonlinear parameter for permeability, ϕ: osmotic coefficient, *FCD*: fixed charge density, D_{free}: ion diffusivity in water, *D*: ion diffusivity within tissue, and *S*: ion solubility.

Solid phase		Fluid phase	
E_m (MPa)	.025	k_0 (mm^4/(Ns))	0.0064
ν (unitless)	0.16	M(unitless)	4.8
β (unitless)	3.3	φ (unitless)	0.938
E_f^* (MPa)	46	FCD(mmol/L)	100
γ (unitless)	4.5	D_{free} (mm^2/s)	0.00147
I_0 (unitless)	1.06^2	D(mm^2/s)	0.0008
ϕ_0 (unitless)	0.3	S(unitless)	1

deformation gradient tensor, **F** (J = det(**F**)), and λ and μ are the Lamé coefficients, which are related to the Young's modulus and Poisson's ratio.

Fibers were defined using a nonlinear stress-stretch relationship with a defined toe- and linear-region separated by a squared transition stretch, I_0 (Eqs. 5–8) (O'Connell et al., 2009). In Eq. (5), γ described the toe-region nonlinearity (unitless), the invariant I_n represented squared fiber stretch (I_n = **a**•**C**•**a**, where **a** is the unit vector that described the fiber orientation in the reference configuration), and E_f represented the linear-region elastic modulus (MPa, constant). In this expression, γ, I_0, and E_f were independent coefficients selected from our previous model, which was calibrated to experimental data from the outer AF (Table 2) (Yang and O'Connell, 2017). E_f was divided in half for models with two-fiber families, such that the total fiber stiffness within a layer remained constant. In Series III, a 20-fold increase in E_f was simulated based on differences in tensile stiffness between tendons or ligaments and the outer AF (tendons/ligament modulus ~ 1 GPa, outer AF modulus ~ 50 MPa) (Holzapfel et al., 2005; Martin et al., 2015). All fibers were limited to acting only in tension.

$$W_{fiber} = \begin{cases} 0 & I_n < 1 \\ \frac{\xi}{2\gamma}(I_n - 1)^\gamma & 1 \le I_n \le I_0 \\ E_f\left(I_0^{\frac{1}{2}} - I_n^{\frac{1}{2}}\right) + B(I_n - I_0) + W_0 & I_0 \le I_n \end{cases} \quad (5)$$

$$\xi = \frac{E_f}{2(\gamma-1)} I_0^{2-\gamma} \quad (6)$$

$$B = \frac{E_f}{2}\left[\frac{I_0-1}{2(\gamma-1)} + I_0\right] \quad (7)$$

$$W_0 = \frac{\xi}{2\gamma}(I_0-1)^\gamma \quad (8)$$

In triphasic theory, negative fixed charge density (FCD) in the solid description was used to represent GAGs in the extrafibrillar matrix by assuming 2 mol of charge per mole of GAG in the tissue and a molecular weight of 502.5 g/mole GAG (Eq. (9)) (Jackson et al., 2009). An initial FCD of − 100 mmol/L was chosen to represent the outer AF GAG content (Urban and Maroudas, 1979). Total fix charges was conserved; therefore, the local FCD (FCD_l) depended on changes in local volume (Eq. (10), where ϕ_0 was tissue solid fraction in the reference configuration, Table 2).

$$FCD_0 = \frac{2 \quad mmol\ charges}{0.5025 \quad g\,GAG} \frac{W_{GAG}}{1 \quad L} \quad (9)$$

$$FCD_l = \frac{1-\phi_0}{J-\phi_0} FCD_0 \quad (10)$$

Fluid (*i.e.*, water) and ion phases were included to simulate tissue swelling (Table 2) (Stadie and Sunderman, 1931; Yasuda et al., 1968). The FCD affected fluid and ions movement by altering the electrochemical potential. Free diffusivity (D_{free}) and diffusivity (*D*) were used to describe time-dependent ion diffusion in water and through the tissue. Permeability (*k*) was used to describe fluid flow through the tissue. Tissue permeability was strain-dependent, and the parameters k_0 and M were selected based on experimental data of the AF (Holmes-Mow permeability model; Eq. (11); Table 2) (Cortes et al., 2014). Diffusivity and permeability only affected time-dependent movement of fluid and ions however steady state was not affected by these parameters. An influx of fluid will cause an increase in interstitial fluid pressure, which results in matrix swelling.

$$k(J) = k_0\left(\frac{J-\phi_0}{1-\phi_0}\right)^2 e^{1/2M(J^2-1)} \quad (11)$$

2.3. Simulation, model validation, and data analyses

All simulations were conducted in FEBio (Maas et al., 2012). Boundary conditions for all models were set such that one end was fixed, while the opposite end was allowed to freely elongate and rotate.

The reference configuration represented a state of osmotic dehydration, where FCD was set to 0. The steady-state swelling was simulated by increasing the magnitude of the FCD from zero to the specified value (−100 mmol/mL) in one second, while the surrounding environment was fixed at a value representing 0.15 M phosphate buffered saline (150 mmol/L). It should be noted tissue-level experiments may allow the annulus fibrosus samples to soak in saline for 30–60 min to reach a steady state condition (Bezci et al., 2015; O'Connell et al., 2009; Żak and Pezowicz, 2016).

Deformations caused by the free-swelling conditions were measured and recorded. The swelling ratio was calculated as the volume in the deformed condition divided by the volume in the reference configuration. Fiber stretch and fiber reorientation were calculated for each element. Briefly, the unit fiber vector (a') in the deformed state was defined as the deformation gradient tensor **F** acting upon the unit fiber vector (**a**) in the reference (**a'** = **Fa**). Fiber stretch was calculated as |**a'**| divided by |**a**|, and fiber reorientation was determined by calculating the angle between **a'** and **a**. In addition, first principal strains (ε_1) were calculated for each element. Fiber stretch, fiber reorientation and fist principal strains were averaged for all elements within the simulated tissue to calculate average fiber stretch, average fiber reorientation, and average first principal strain, respectively. Only fibers under tensile stretch were included in the calculation for average fiber stretch. Finally, swelling ratio was correlated with average fiber stretch and first principal strain.

To validate model simulations, changes in dimensions and volume for the 6-layer model with fibers oriented at ± 60° in Series I (control model) were compared to free swelling experiments of AF explants from bovine discs (Bezci et al., 2015; Żak and Pezowicz, 2016). Model results were considered valid if changes in length, width, thickness, and volume fell within the range of data reported in the literature.

3. Results

3.1. Model validation

The volume of the 6-layer model with fibers oriented at ± 60° (control model) increased by 46% under free-swelling conditions, which was within the wide range of values reported in the literature (20 − 70%) (Bezci et al., 2015; Żak and Pezowicz, 2016). Swelling of the control model resulted in a 27% increase in thickness and a 15% increase in length, which was comparable to respective increases in length along the radial (21 ± 4%) and axial directions (14 ± 6%) of the AF (Żak and Pezowicz, 2016). Furthermore, the control model had a − 3% change in width, which agreed with change in circumferential direction length of AF explants during swelling (−2 ± 4%). Since model results were within one standard deviation of reported mean values for three of the four parameters (changes in volume, width, and thickness) and within two standard deviations of the mean for the change in length, we considered the model to be valid for studying swelling behavior of fiber-reinforced tissues.

3.2. Swelling ratio

The 'No Fiber' model, which represents the extrafibrillar matrix without fibers, had a 62% increase in tissue volume under free-swelling conditions (swelling ratio = 1.62; Figs. 2–4 & Fig. 5 - black solid line). For models in Series I, adding fibers to single-layer models decreased tissue swelling by ~ 10%, and the decrease in swelling ratio was consistent, regardless of fiber orientation (swelling ratio = 1.52; Fig. 2A, Fig. 5 – solid light blue line). For 2-layer models in Series I, the swelling ratio was dependent on fiber orientation, as the cross-ply fiber architecture further reduced tissue swelling (swelling ratio = 1.44 for the ± 45° model; Fig. 2B & Fig. 5 – solid purple line). There was a nonlinear relationship between the decrease in swelling ratio and the number of lamellae included. That is, the swelling ratio for multi-lamella structures was comparable for tissues with three or more lamellae (Fig. 2C-E; Fig. 5 - inset).

As expected, the two-fiber family structure used in Series II models eliminated any effect of multi-lamella architecture on swelling behavior. As such, 2- and 3-layer models exhibited the same response (Fig. 4). Multi-lamellae models in Series II did not exhibit signs of rotation or twisting and the swelling ratio was uniform throughout the material (Fig. 3). Two-fiber family structure Tissue swelling decreased tissue swelling capacity, with the largest difference observed in models with fibers orientated at ± 45° (from 1.45 to 1.40; Fig. 5-purple dashed line verses respective models from Series I: solid purple line for 2-layers and solid red line for 3-layers). Fiber stiffness had a minor influence on swelling ratio (Fig. 4), where a 20-fold increase in fiber stiffness resulted in less than a 2% reduction in swelling ratio (Fig. 5 - solid gray line *versus* solid red line and gray dashed line *versus* purple dashed line).

3.3. Swelling deformation and first principal strain

Dimensions of the 'No Fiber' models increased uniformly in all directions (17.3% increase in length, width, and thickness). Elongation along the z-direction was observed for all 1-layer models in Series I (Fig. 2A), but z-direction elongation depended on fiber orientation in multi-lamellae models (Series I-III; Figs. 2B-E, 3 & 4). That is, minimal tissue elongation was observed for models with fibers oriented between 0° and ± 45° (< 3.5% of original length), while tissue elongation was up to 22% of the original length for models with fibers oriented between ± 45° and ± 90° (Figs. 2–4).

The increase in tissue thickness (*i.e.*, orientation perpendicular to fibers) was greater than 25% for all fiber-reinforced models. Similarly, strains were greatest in the orientation perpendicular to the fibers, and, therefore, was the direction of the first principal strain (Fig. 6A). In Series I, the first principal strain for 1-layer models was consistent, regardless of fiber orientation (ε_1 = 0.25; Fig. 6A – light blue). For all other models in Series I (*i.e.*, multi-lamellae models), the average first principal strain depended on fiber orientation, where the ± 45° models exhibited the largest average first principal strains (Fig. 6A). There were little differences in average first principle strain for multi-lamellae models in Series I and for models from Series II or III (*i.e.*, with respect to multi-fiber families or fiber stiffness, Fig. 6A – *e.g.*, solid red line verses purple or gray lines).

Tissue rotation or twisting was observed in single and multi-lamella models from Series I. Single layer models (1-layer models) rotated about the y-axis, which was the axis perpendicular to the fibers (Fig. 2A), resulting in shear strains in the xz plane (ε_{xz} (θ), Fig. 6B). Multi-lamella models with an even number of layers in Series I resulted in rotation about the z-axis (Fig. 2B). The amount of rotation depended on fiber orientation, where maximum rotation occurred for models with fibers oriented at ~ ± 45° (Fig. 2B). Twisting about the z-axis decreased as the number of lamellae increased from two to six layers. That is, the rotation angle for the ± 45° model decreased from 187° in the 2-layer model to 26° and 22° in the 4- and 6-layer models, respectively (Fig. 2B, D, and E).

3.4. Fiber stretch and reorientation

Swelling caused fiber deformations, which were reported as fiber stretch. The magnitude of fiber stretch was consistent for all 1-layer models in Series I (fiber stretch = 1.02; Fig. 7A). The average fiber stretch was comparable between 1- and 2-layer models in Series I (Fig. 7A – purple line *versus* light blue line). However, for models with three or more layers, the fiber stretch depended on fiber orientation, where models with fibers orientated at ± 45° had the greatest fiber deformations (Fig. 7A - solid red, dark blue, green, and gray lines). Models in Series II experienced higher fiber deformations than Series I models, and this difference was more pronounced for the 2-layer cases (Fig. 7A - solid *versus* dashed purple line). For models in Series III, an

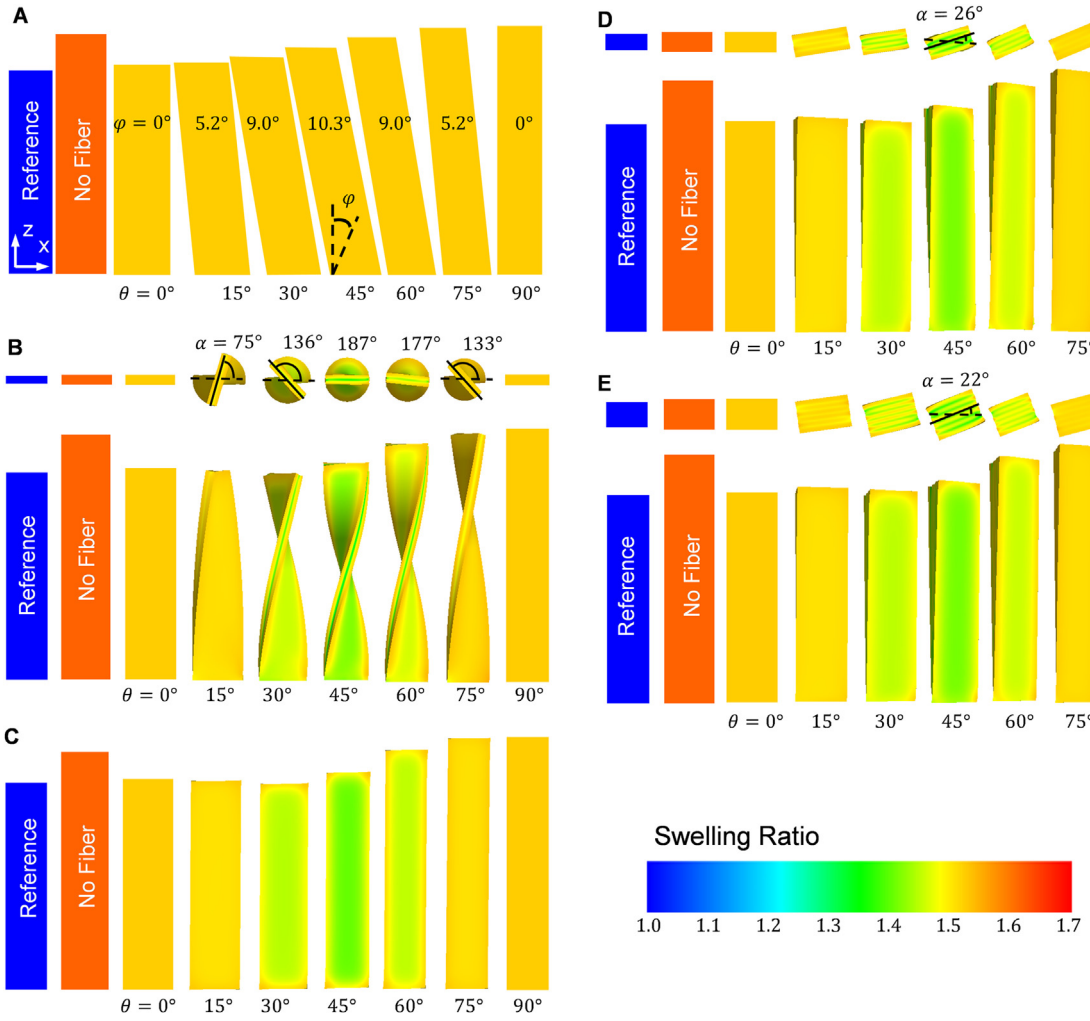

Fig. 2. Configurations for models in Series I before ('Reference' configuration) and after swelling: 1-layer (A), 2-layer (B), 3-layer (C), 4-layer (D), and 6-layer (E) models. The color bar represents swelling ratio, which was defined as the volume after swelling divided by the volume before swelling. φ represents fiber reorientation angle about the y-axis and α represents tissue rotation angle about the z-axis.

increase in fiber stiffness decreased fiber deformations by ~ 50% for all fiber orientations (Fig. 7A - gray lines).

Free swelling conditions caused fibers to reorient either towards (negative change in fiber angle) or away from the z-axis. For Series I models, rotations about the y-axis were observed in 1-layer models, resulting in fibers reorienting away from the z-axis (Fig. 2A; Fig. 7B - light blue solid line). Fiber reorientation response was relatively consistent for all other models (Series I-III), and the direction of fiber reorientation depended on the initial fiber orientation. That is, models with fibers initially orientated between 0 and ± 45° reoriented away from the z-axis, while fibers that were initially oriented at > ± 45° reoriented towards the longitudinal or z-axis (Fig. 7B).

3.5. Relationship between swelling ratio and fiber deformations

Lastly, we looked at the relationship between swelling ratio and fiber deformations for each fiber network configuration. There was a negative linear relationship between swelling ratio and average fiber stretch (Fig. 8A). The decrease in tissue swelling with respect to fiber stretch was more pronounced for models with stiffer fibers (Fig. 8A – gray lines for Series III *versus* multi-colored lines for Series I and II). Similarly, there was a negative linear relationship between swelling ratio and average first principal strain (Fig. 8B). The decrease in swelling ratio with respect to the average first principal strain was consistent for all fiber network configurations (Series I-III, slope = ~ −0.94; Fig. 8B).

4. Discussion

Our previous work and work by others showed that tissue hydration affects tissue- and joint-level mechanics (Bezci and O'Connell, 2017; Bezci et al., 2015; Żak and Pezowicz, 2016). Our previous experimental studies showed that the AF swelling capacity was ~ 70% of the nucleus pulposus. However, it was difficult to discern whether differences in swelling capacity was entirely due to differences in glycosaminoglycan composition or differences in fiber network, as recent work showed anisotropic swelling behavior in the AF (Żak and Pezowicz, 2016). Therefore, in this study, we developed three series of finite element models to evaluate the effect of collagen fiber orientation (Series I), fiber network architecture (Series I & II), and fiber stiffness (Series III) on tissue swelling. The model was validated by comparing simulated swelling response with experimental results from AF explants (Bezci et al., 2015; Żak and Pezowicz, 2016). Simulations from these models showed that fiber angle, fiber architecture, and the number of lamellae in single fiber-family structures alters tissue swelling capacity, fiber deformation, and tissue rotation.

Accurate characterization of healthy and diseased biological tissues is important for developing materials for repairing or replacing damaged and diseased tissues. Ideally, replacement materials will mimic the mechanical function of the healthy native tissue, but the mechanical

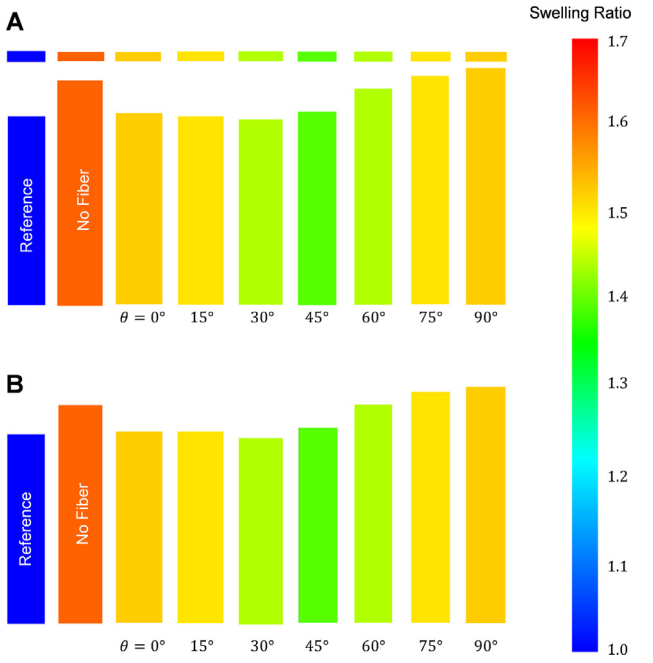

Fig. 3. Configurations for models in Series II before ('Reference' configuration) and after swelling: 2-layer, 2 fiber family (A) and 3-layer 2-fiber family (B) descriptions. Swelling behavior was not dependent on the number of lamella within a tissue when a multiple fiber family description was used. Color map represents the swelling ratio.

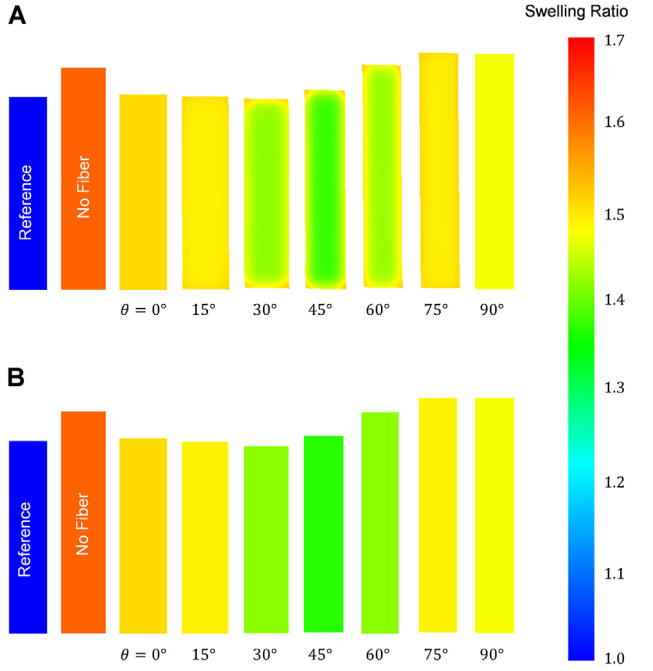

Fig. 4. Configurations for models in Series III before ('Reference' configuration) and after swelling: 3-layer model with stiffer fibers (A) and 3-layer 2 fiber family description with stiffer fibers (B). There was a slight decrease in swelling ratio with fiber stiffness (compared to Figs. 2C and 3B, respectively). Color map represents the swelling ratio.

properties (*e.g.,* Young's modulus) of biological tissues are highly dependent on hydration condition (Galante, 1967; Panagiotacopulos et al., 1979; Skaggs et al., 1994; Żak and Pezowicz, 2016). The largest dimensional increase observed in this study occurred in the thickness direction, which would greatly affect the cross-sectional area and,

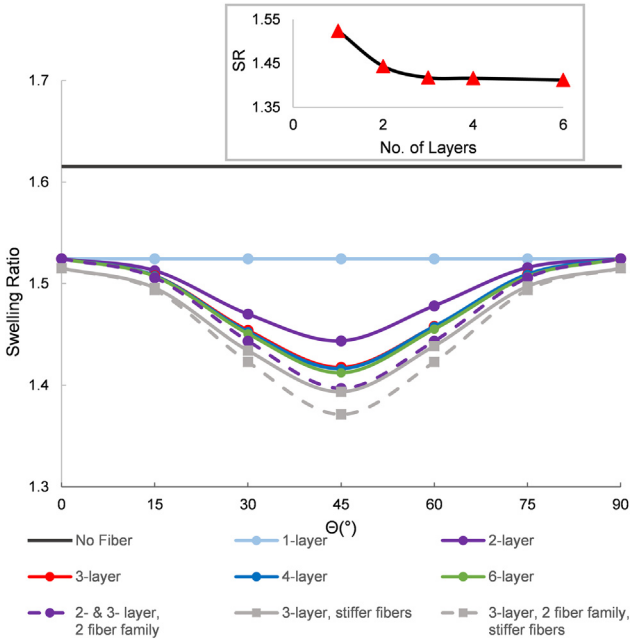

Fig. 5. Swelling ratio (SR) with respect to initial fiber orientation for all models in Series I, II, and III. *Inset:* Swelling ratio with respect to the number of layers in Series I. ***Note*** **–** Values on the y-axis do not start at 1.0 (*i.e.,* case with no swelling in the tissue).

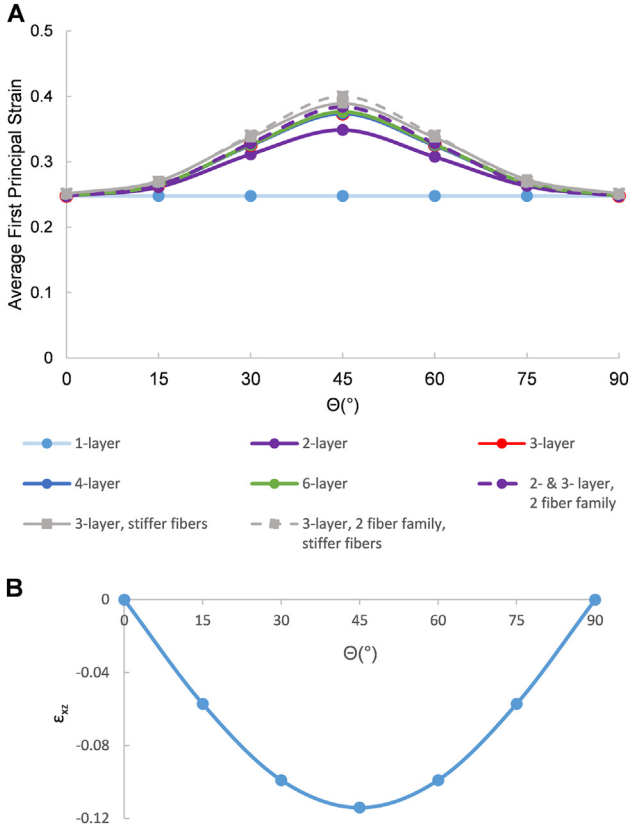

Fig. 6. Average first principal strain with respect to the initial fiber orientation for all models (A). In-plane shear strain (ε_{xz}) for 1-layer models in Series I with respect to fiber orientation (B).

therefore, stress and modulus calculations. Some of the differences in mechanical properties reported in the literature have been attributed to changes in cross-sectional area (Han et al., 2012). However, other

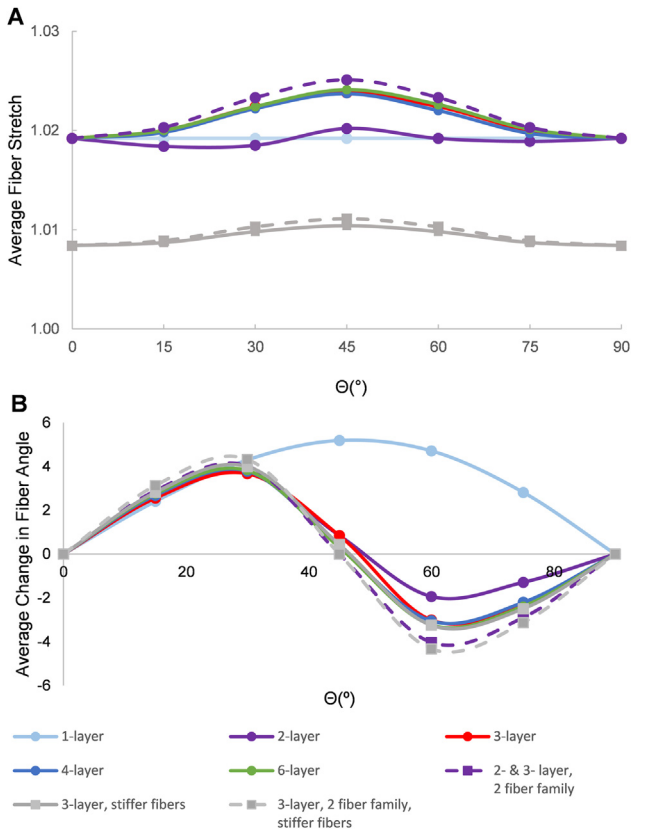

Fig. 7. Average fiber stretch due to swelling with respect to the initial fiber orientation for all models (A) and average change in fiber orientation with swelling (B).

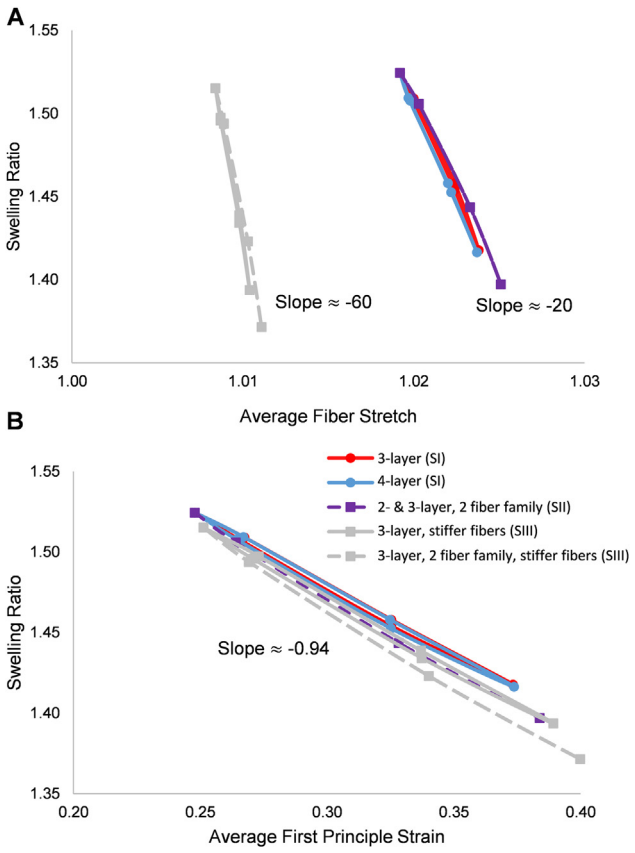

Fig. 8. Swelling ratio with respect to the average fiber stretch (A) and swelling ratio with respect to the average first principal strain (B) for models from all three network configurations (SI = Series I, SII = Series II, and SIII = Series III).

studies suggest that changes in tissue mechanics are also due to non-geometric tissue changes (Narmoneva et al., 2002; Żak and Pezowicz, 2016). The findings from this study agree with that notion and suggest that fiber rotation may be responsible in part for non-geometric changes that lead to differences in material properties (Fig. 7A).

Fiber reorientation and uncrimping act to reduce stresses on collagen fibrils during tensile loading (Tower et al., 2002). In this study, we observed greater fiber reorientation and fiber stretch in models that represented AF anatomy, compared to models that more closely represent tendon anatomy (*i.e.*, AF anatomy: ~ ± 5° fiber rotation and average fiber stretch ~ 1.023; tendon anatomy: no fiber rotation and average fiber stretch ~ 1.019; Fig. 7). Previous experimental studies on AF and tendon mechanics demonstrated fiber reorientation towards the direction of tensile loading (Guerin and Elliott, 2006; Lake et al., 2009). Guerin *et al.* reported that fibers realigned by 5° towards the loading direction under tissue strains between 4% and 6% (*i.e.*, stretch = 1.02–1.03) (Guerin and Elliott, 2006). Taken together, fiber reorientation during swelling may contribute to the pronounced toe-region observed in AF tissues, which is not as pronounced in stress-strain curves of more aligned tissues, such as tendons or ligaments, or AF specimens tested in air (Galante, 1967; Hansen et al., 2002; O'Connell et al., 2009; Skaggs et al., 1994;).

Tissue swelling was due to a balance between matrix swelling and fiber stretch. Tendons and ligaments have a higher collagen content and a lower GAG content than the outer AF (collagen: 80% *versus* 70% per dry weight, GAG: < 3% verses 10% per dry weight, respectively). Moreover, collagen fibrils in tendons and ligaments are more aligned and stiffer than fibrils from the AF (Cassidy et al., 1989; Lynch et al., 2003). These differences in tissue composition are related to a limited overall swelling capacity (~ 10% increase in tendon volume in saline verses ~ 40% increase in AF volume) (Adams, 2004; Amiel et al., 1983; Henninger et al., 2010; Iatridis et al., 2007; Riley et al., 1994; Safa et al., 2017). Our findings showed that tissues with fibers aligned in a single direction (*i.e.*, no cross-ply pattern) have less ability to resist matrix swelling. In contrast, fibers in a cross-ply configuration are effective in resisting matrix swelling, resulting in greater fiber stretch. Therefore, tissues with fibers aligned along a single direction (*i.e.,* 0° or 90°) would need stiffer fibers or fewer GAGs to reduce matrix swelling and achieve the same swelling capacity as tissues with a cross-ply architecture, which agrees with biochemical differences between tendons and AF.

Tissue twisting about the z-axis was observed in a subset of models in Series I, specifically, in models with an even number of lamellae. Twisting or curling has been observed in maturing electrospun constructs (thickness = 0.56 – 0.9 mm) (Baker et al., 2008); however, it is difficult to separate curling due to cell contraction from matrix swelling (Tan et al., 2003). Recent analytical work also observed specimen twisting when simulating swelling in a hollow cylinder comprised of curved fibers along the radial direction (Demirkoparan and Pence, 2017). Twisting has not been widely reported for native fiber-reinforced materials, which may be due to test specimens containing more than four lamellae (twisting angle < 25°) or the application of a nominal preload to ensure specimen alignment prior to mechanical testing (Guerin and Elliott, 2007; O'Connell et al., 2009). The decrease in tissue rotation with additional lamella was likely due to opposing rotation angles in adjacent layers (Fig. 9). These findings agree with work by Nerukar *et al.* that observed high shear stresses between cross-ply lamellae, which led to an increase in bulk tissue stiffness in engineered fiber-reinforced tissues (Nerurkar et al., 2011).

The two fiber family description is a more commonly used fiber description for computational models of fiber-reinforced materials

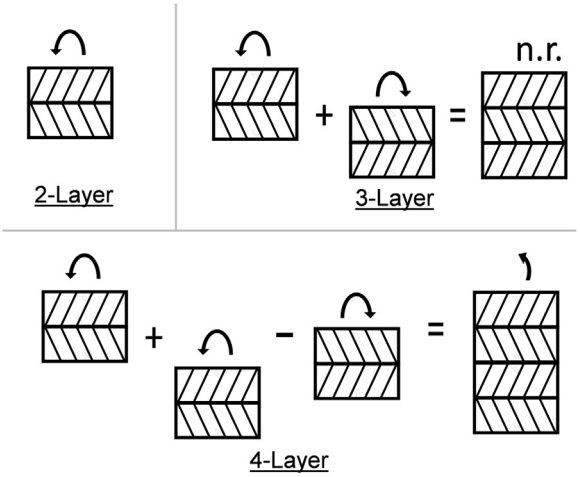

Fig. 9. Schematic of twisting for 2-, 3-, and 4-layer rectangular models with cross-ply fiber description. Models with an odd number of lamellae did not experience twisting due to opposing rotations between layers (n.r. = no rotation).

(Holzapfel et al., 2000; Roccabianca et al., 2014; Schmidt et al., 2006; Shirazi-Adl et al., 1984; Yang and O'Connell, 2017), but the alternating single fiber family description more closely aligns with the native fiber network of the AF and media of vascular walls (Cassidy et al., 1989; Marchand and Ahmed, 1990; Rhodin, 2011; Timmins et al., 2010). Our findings showed that bulk tissue swelling behavior was dependent on the fiber architecture description, especially in tissues with less than three layers. That is, the two-fiber family description had lower predicted increases in volume (Figs. 3 & 4B), more uniform swelling distribution, and did not exhibit signs of twisting or rotation (Fig. 2 *versus* 3). Therefore, as computational models shift from describing the extrafibrillar matrix as a hyperelastic material to a material with fluid-dependent behaviors (*e.g.*, biphasic or triphasic descriptions) (Ateshian et al., 2004; Schmidt et al., 2013), an accurate description of the fiber architecture will become essential for predicting internal stresses and strains that may lead to damage.

There are some limitations to the current study. GAGs are the primary contributor to tissue swelling behavior; however, the effect negative charge density (*i.e.*, GAG composition) on swelling of fiber-reinforced soft tissue was not investigated in this study to focus model simulations on understanding the role of the fiber network on tissue swelling. Although lamellae fibers and fiber dispersion have been observed (Cortes et al., 2010; Schollum et al., 2009), these properties were not included in the models for computational simplicity. Secondly, all models were described using a homogenized material description, where each element is occupied by both a fiber and matrix description, which is not representative of the native tissue. Moreover, we used a rectangular geometry, based on uniaxial test specimens to compare differences due to fiber orientation; however, *in situ* boundary conditions, such as a circular ring for arteries or the kidney shape for the AF, may lead to more complex stress and strain distributions that may affect overall tissue swelling (Azeloglu et al., 2008; Michalek et al., 2012). Finally, material properties were tuned to experimental data from the AF, which may affect swelling ratio and fiber stretch values calculated for non-AF tissues.

Developing constitutive models with an accurate description of the fiber network and swelling behavior of the extrafibrillar matrix is important for designing replacement materials that recapitulate the mechanical function of the native tissue. For example, tensile stiffness increases with more aligned fibers (*e.g.*, from ± 45° to 0°) and shear modulus increases as the fiber orientation approaches ± 45° (Driscoll et al., 2011; Guerin and Elliott, 2006; Jacobs et al., 2011; Yin and Elliott, 2004). The findings of this study demonstrate the need to include the native fiber network in computational models to accurately simulate tissue-swelling behavior, and, therefore, subfailure and failure mechanics. In conclusion, fiber architecture including fiber orientation and lamellae structure had the greatest impact on the swelling capacity of fiber-reinforced tissues. Future work will expand upon this work by evaluating interactions between fiber network and GAG composition on tissue swelling. As swelling could affect mechanical properties of fiber-reinforced soft tissue, estimations of these effects will also be focus of future work.

Competing interests

We have no competing interests.

Authors' contributions

Bo Yang and Grace D. O'Connell participated in study design, data analysis, data interpretation, and manuscript writing. Both authors provided final approval for publication. The authors would like to thank Minhao Zhou for his help with running some of the simulations reported in this study.

Funding

This work was supported by the Helman Foundation, a Block Grant Award, and J. K. Zee Fellowship from the University of California - Berkeley Graduate Division.

References

Abazari, A., Elliott, J.A., Law, G.K., McGann, L.E., Jomha, N.M., 2009. A biomechanical triphasic approach to the transport of nondilute solutions in articular cartilage. Biophys. J. 97, 3054–3064.
Abraham, A.C., Edwards, C.R., Odegard, G.M., Donahue, T.L., 2011. Regional and fiber orientation dependent shear properties and anisotropy of bovine meniscus. J. Mech. Behav. Biomed. Mater. 4, 2024–2030.
Acaroglu, E.R., Iatridis, J.C., Setton, L.A., Foster, R.J., Mow, V.C., Weidenbaum, M., 1995. Degeneration and aging affect the tensile behavior of human lumbar anulus fibrosus. Spine 20, 2690–2701.
Adams, M.A., 2004. Biomechanics of back pain. Acupunct. Med. 22, 178–188.
Amiel, D., Frank, C., Harwood, F., Fronek, J., Akeson, W., 1983. Tendons and ligaments: a morphological and biochemical comparison. J. Orthop. Res. 1, 257–265.
Ateshian, G.A., Chahine, N.O., Basalo, I.M., Hung, C.T., 2004. The correspondence between equilibrium biphasic and triphasic material properties in mixture models of articular cartilage. J. Biomech. 37, 391–400.
Azeloglu, E.U., Albro, M.B., Thimmappa, V.A., Ateshian, G.A., Costa, K.D., 2008. Heterogeneous transmural proteoglycan distribution provides a mechanism for regulating residual stresses in the aorta. Am. J. Physiol.-Heart Circ. Physiol. 294, H1197–H1205.
Baker, B.M., Gee, A.O., Metter, R.B., Nathan, A.S., Marklein, R.A., Burdick, J.A., Mauck, R.L., 2008. The potential to improve cell infiltration in composite fiber-aligned electrospun scaffolds by the selective removal of sacrificial fibers. Biomaterials 29, 2348–2358.
Bezci, S., O'Connell, G., 2017. Osmotic Pressure Alters Time-dependent Recovery Behavior of the Intervertebral Disc. Spine.
Bezci, S.E., Nandy, A., O'Connell, G.D., 2015. Effect of hydration on healthy intervertebral disk mechanical stiffness. J. Biomech. Eng. 137, 101007.
Cassidy, J., Hiltner, A., Baer, E., 1989. Hierarchical structure of the intervertebral disc. Connect. Tissue Res. 23, 75–88.
Cortes, D.H., Elliott, D.M., 2012. Extra-fibrillar matrix mechanics of annulus fibrosus in tension and compression. Biomech. Model. Mechanobiol. 11, 781–790.
Cortes, D.H., Lake, S.P., Kadlowec, J.A., Soslowsky, L.J., Elliott, D.M., 2010. Characterizing the mechanical contribution of fiber angular distribution in connective tissue: comparison of two modeling approaches. Biomech. Model. Mechanobiol. 9, 651–658.
Cortes, D.H., Jacobs, N.T., DeLucca, J.F., Elliott, D.M., 2014. Elastic, permeability and swelling properties of human intervertebral disc tissues: a benchmark for tissue engineering. J. Biomech. 47, 2088–2094.
Demirkoparan, H., Pence, T.J., 2017. Swelling–twist interaction in fiber-reinforced hyperelastic materials: the example of azimuthal shear. J. Eng. Math. 1–22.
Driscoll, T.P., Nerurkar, N.L., Jacobs, N.T., Elliott, D.M., Mauck, R.L., 2011. Fiber angle and aspect ratio influence the shear mechanics of oriented electrospun nanofibrous scaffolds. J. Mech. Behav. Biomed. Mater. 4, 1627–1636.
Elliott, D.M., Setton, L.A., 2001. Anisotropic and inhomogeneous tensile behavior of the human anulus fibrosus: experimental measurement and material model predictions. J. Biomech. Eng. 123, 256–263.

Eyre, D.R., Muir, H., 1976. Types I and II collagens in intervertebral disc. Interchanging radial distributions in annulus fibrosus. Biochem. J. 157, 267–270.
Fung, Y., 1991. What are the residual stresses doing in our blood vessels? Ann. Biomed. Eng. 19, 237–249.
Galante, J.O., 1967. Tensile properties of the human lumbar annulus fibrosus. Acta Orthop. Scand. 38 (sup100), 1–91.
Green, T., Adams, M., Dolan, P., 1993. Tensile properties of the annulus fibrosus. Eur. Spine J. 2, 209–214.
Guerin, H.A.L., Elliott, D.M., 2006. Degeneration affects the fiber reorientation of human annulus fibrosus under tensile load. J. Biomech. 39, 1410–1418.
Guerin, H.L., Elliott, D.M., 2007. Quantifying the contributions of structure to annulus fibrosus mechanical function using a nonlinear, anisotropic, hyperelastic model. J. Orthop. Res. 25, 508–516.
Han, W.M., Nerurkar, N.L., Smith, L.J., Jacobs, N.T., Mauck, R.L., Elliott, D.M., 2012. Multi-scale structural and tensile mechanical response of annulus fibrosus to osmotic loading. Ann. Biomed. Eng. 40, 1610–1621.
Hansen, K.A., Weiss, J.A., Barton, J.K., 2002. Recruitment of tendon crimp with applied tensile strain. J. Biomech. Eng. 124, 72–77.
Henninger, H.B., Underwood, C.J., Ateshian, G.A., Weiss, J.A., 2010. Effect of sulfated glycosaminoglycan digestion on the transverse permeability of medial collateral ligament. J. Biomech. 43, 2567–2573.
Holzapfel, G.A., Gasser, T.C., Ogden, R.W., 2000. A new constitutive framework for arterial wall mechanics and a comparative study of material models. J. Elast. Phys. Sci. Solids 61, 1–48.
Holzapfel, G.A., Schulze-Bauer, C., Feigl, G., Regitnig, P., 2005. Single lamellar mechanics of the human lumbar anulus fibrosus. Biomech. Model. Mechanobiol. 3, 125–140.
Iatridis, J.C., MacLean, J.J., O'Brien, M., Stokes, I.A., 2007. Measurements of proteoglycan and water content distribution in human lumbar intervertebral discs. Spine 32, 1493.
Jackson, A.R., Yuan, T.Y., Huang, C.Y., Gu, W.Y., 2009. A conductivity approach to measuring fixed charge density in intervertebral disc tissue. Ann. Biomed. Eng. 37 (12), 2566–2573.
Jacobs, N.T., Smith, L.J., Han, W.M., Morelli, J., Yoder, J.H., Elliott, D.M., 2011. Effect of orientation and targeted extracellular matrix degradation on the shear mechanical properties of the annulus fibrosus. J. Mech. Behav. Biomed. Mater. 4, 1611–1619.
Kannus, P., 2000. Structure of the tendon connective tissue. Scand. J. Med. Sci. Sports 10, 312–320.
Lai, W.M., Hou, J., Mow, V.C., 1991. A triphasic theory for the swelling and deformation behaviors of articular cartilage. J. Biomech. Eng. 113, 245–258.
Lake, S.P., Miller, K.S., Elliott, D.M., Soslowsky, L.J., 2009. Effect of fiber distribution and realignment on the nonlinear and inhomogeneous mechanical properties of human supraspinatus tendon under longitudinal tensile loading. J. Orthop. Res. 27, 1596–1602.
Lemaitre, J., 2001. Handbook of Materials Behavior Models, Three-Volume Set: Nonlinear Models and Properties. Elsevier.
Lin, T.W., Cardenas, L., Soslowsky, L.J., 2004. Biomechanics of tendon injury and repair. J. Biomech. 37, 865–877.
Lynch, H.A., Johannessen, W., Wu, J.P., Jawa, A., Elliott, D.M., 2003. Effect of fiber orientation and strain rate on the nonlinear uniaxial tensile material properties of tendon. J. Biomech. Eng. 125, 726–731.
Maas, S.A., Ellis, B.J., Ateshian, G.A., Weiss, J.A., 2012. FEBio: finite elements for biomechanics. J. Biomech. Eng. 134, 011005.
Marchand, F., Ahmed, A.M., 1990. Investigation of the laminate structure of lumbar disc anulus fibrosus. Spine 15, 402–410.
Martin, R.B., Burr, D.B., Sharkey, N.A., Fyhrie, D.P., 2015. Mechanical properties of ligament and tendon. In: Skeletal Tissue Mechanics. Springer, pp. 175–225.
Meng, Q., An, S., Damion, R.A., Jin, Z., Wilcox, R., Fisher, J., Jones, A., 2017. The effect of collagen fibril orientation on the biphasic mechanics of articular cartilage. J. Mech. Behav. Biomed. Mater. 65, 439–453.
Michalek, A., Gardner-Morse, M., Iatridis, J., 2012. Large residual strains are present in the intervertebral disc annulus fibrosus in the unloaded state. J. Biomech. 45, 1227–1231.
Narmoneva, D.A., Cheung, H.S., Wang, J.Y., Howell, D.S., Setton, L.A., 2002. Altered swelling behavior of femoral cartilage following joint immobilization in a canine model. J. Orthop. Res. 20, 83–91.
Nerurkar, N.L., Mauck, R.L., Elliott, D.M., 2011. Modeling interlamellar interactions in angle-ply biologic laminates for annulus fibrosus tissue engineering. Biomech. Model. Mechanobiol. 10, 973–984.
O'Connell, G.D., Guerin, H.L., Elliott, D.M., 2009. Theoretical and uniaxial experimental evaluation of human annulus fibrosus degeneration. J. Biomech. Eng. 131, 111007.
O'Connell, G.D., Sen, S., Elliott, D.M., 2012. Human annulus fibrosus material properties from biaxial testing and constitutive modeling are altered with degeneration. Biomech. Model. Mechanobiol. 11, 493–503.
Panagiotacopulos, N., Knauss, W., Bloch, R., 1979. On the mechanical properties of human intervertebral disc material. Biorheology 16, 317–330.
Rhodin, J.A., 2011. Architecture of the vessel wall. Comprehensive Physiology.
Riley, G., Harrall, R., Constant, C., Chard, M., Cawston, T., Hazleman, B., 1994. Glycosaminoglycans of human rotator cuff tendons: changes with age and in chronic rotator cuff tendinitis. Ann. Rheum. Dis. 53, 367–376.
Roccabianca, S., Bellini, C., Humphrey, J., 2014. Computational modelling suggests good, bad and ugly roles of glycosaminoglycans in arterial wall mechanics and mechanobiology. J. R. Soc. Interface 11, 20140397.
Rumian, A.P., Wallace, A.L., Birch, H.L., 2007. Tendons and ligaments are anatomically distinct but overlap in molecular and morphological features—a comparative study in an ovine model. J. Orthop. Res. 25, 458–464.
Safa, B.N., Meadows, K.D., Szczesny, S.E., Elliott, D.M., 2017. Exposure to buffer solution alters tendon hydration and mechanics. J. Biomech. 61, 18–25.
Schmidt, H., Heuer, F., Simon, U., Kettler, A., Rohlmann, A., Claes, L., Wilke, H.-J., 2006. Application of a new calibration method for a three-dimensional finite element model of a human lumbar annulus fibrosus. Clin. Biomech. 21, 337–344.
Schmidt, H., Galbusera, F., Rohlmann, A., Shirazi-Adl, A., 2013. What have we learned from finite element model studies of lumbar intervertebral discs in the past four decades? J. Biomech. 46, 2342–2355.
Schollum, M.L., Robertson, P.A., Broom, N.D., 2009. A microstructural investigation of intervertebral disc lamellar connectivity: detailed analysis of the translamellar bridges. J. Anat. 214, 805–816.
Screen, H.R., Chhaya, V.H., Greenwald, S.E., Bader, D.L., Lee, D.A., Shelton, J.C., 2006. The influence of swelling and matrix degradation on the microstructural integrity of tendon. Acta Biomater. 2, 505–513.
Shirazi, R., Shirazi-Adl, A., 2008. Deep vertical collagen fibrils play a significant role in mechanics of articular cartilage. J. Orthop. Res. 26, 608–615.
Shirazi-Adl, S.A., Shrivastava, S.C., Ahmed, A.M., 1984. Stress analysis of the lumbar disc-body unit in compression. A three-dimensional nonlinear finite element study. Spine 9, 120–134.
Skaggs, D., Weidenbaum, M., Iatridis, J., Ratcliffe, A., Mow, V., 1994. Regional variation in tensile properties and biochemical composition of the human lumbar anulus fibrosus. Spine 19, 1310–1319.
Stadie, W.C., Sunderman, F.W., 1931. The osmotic coefficient of sodium in sodium hemoglobinate and of sodium chloride in hemoglobin solution. J. Biol. Chem. 91, 227–241.
Standard, A., 2004. E8," Standard Test Methods for Tension Testing of Metallic Materials. Annual book of ASTM standards 3. pp. 57–72.
Tan, J.L., Tien, J., Pirone, D.M., Gray, D.S., Bhadriraju, K., Chen, C.S., 2003. Cells lying on a bed of microneedles: an approach to isolate mechanical force. Proc. Natl. Acad. Sci. USA 100, 1484–1489.
Timmins, L.H., Wu, Q., Yeh, A.T., Moore, J.E., Greenwald, S.E., 2010. Structural inhomogeneity and fiber orientation in the inner arterial media. Am. J. Physiol.-Heart Circ. Physiol. 298, H1537–H1545.
Tower, T.T., Neidert, M.R., Tranquillo, R.T., 2002. Fiber alignment imaging during mechanical testing of soft tissues. Ann. Biomed. Eng. 30, 1221–1233.
Urban, J., Maroudas, A., 1979. The measurement of fixed charged density in the intervertebral disc. Biochim. Et. Biophys. Acta (BBA)-General. Subj. 586, 166–178.
Wagner, D.R., Lotz, J.C., 2004. Theoretical model and experimental results for the nonlinear elastic behavior of human annulus fibrosus. J. Orthop. Res. 22, 901–909.
Wang, Y., Zeinali-Davarani, S., Zhang, Y., 2016. Arterial mechanics considering the structural and mechanical contributions of ECM constituents. J. Biomech. 49 (12), 2358–2365.
Wood, M.L., Lester, G.E., Dahners, L.E., 1998. Collagen fiber sliding during ligament growth and contracture. J. Orthop. Res. 16, 438–440.
Yang, B., O'Connell, G.D., 2017. Effect of collagen fibre orientation on intervertebral disc torsion mechanics. Biomech. Model. Mechanobiol. 16, 2005–2015.
Yasuda, H., Lamaze, C., Ikenberry, L., 1968. Permeability of solutes through hydrated polymer membranes. Part I. diffusion of sodium chloride. Macromol. Chem. Phys. 118, 19–35.
Yin, L., Elliott, D.M., 2004. A biphasic and transversely isotropic mechanical model for tendon:: application to mouse tail fascicles in uniaxial tension. J. Biomech. 37, 907–916.
Yoshida, K., Mahendroo, M., Vink, J., Wapner, R., Myers, K., 2016. Material properties of mouse cervical tissue in normal gestation. Acta Biomater. 36, 195–209.
Żak, M., Pezowicz, C., 2016. Analysis of the impact of the course of hydration on the mechanical properties of the annulus fibrosus of the intervertebral disc. Eur. Spine J. 25, 2681–2690.